Riding Stress Wave: Underwater Communications Through Pipeline Networks

Debing Wei, Student Member, IEEE, Chaoxian Qi, Student Member, IEEE, Chenpei Huang, Student Member, IEEE, Jiefu Chen, Senior Member, IEEE, Aijun Song, Gangbing Song, and Miao Pan, Senior Member, IEEE

Abstract—The majority of research works on underwater communications have been struggling against the water medium for a long time. Either acoustic, electromagnetic, or optical waves suffer from specific propagation defects in the water. Briefly, acoustic waves suffer from long propagation delay and frequency-selective fading. Electromagnetic waves are susceptible to the significant attenuation in the conductive seawater. Strong absorption and severe Rayleigh scattering make wireless optical communication vulnerable. Therefore, a reliable, long-range (up to kilometer), and high data-rate (up to megabits per second) wireless communication is still unavailable in the underwater environments so far. Fortunately, in the past few decades, massive offshore pipeline networks have been deployed for oil and gas transportation. These pipelines provide a new medium for realizing underwater communications, in which the acoustic wave propagates in the pipe wall (also known as stress wave). This stress wave assisted communication scheme overcomes some drawbacks within the aforementioned modalities. So, in this article, we propose a brand new underwater communication paradigm, namely underwater stress wave communications, which utilizes stress wave and offshore pipeline networks for underwater data transmission. Fundamentally different from the conventional underwater communication schemes, stress wave signals propagate through the solid pipe instead of water. Therefore, underwater stress wave communications exhibit several unique and promising features, including 1) lower latency and higher bandwidth compared with acoustic communications; 2) longer communication range than electromagnetic and optical communications; and 3) nearly deterministic and constant channel conditions. To fully utilize these promising features to establish reliable, secure, and high-data-rate communication links along offshore pipelines, this article investigates the stress wave channel characteristics including path loss, available bandwidth, and channel response. Furthermore, we demonstrated a stress wave communication along a steel pipe both in the air and water, and experiment results indicated the feasibility of stress-wave-based communications.

Manuscript received June 4, 2020; revised March 19, 2021; accepted May 21, 2021. The work of Debing Wei, Chenpei Huang, Jiefu Chen, Gangbing Song, and Miao Pan was supported by the U.S. National Science Foundation under Grant CNS-1801925. The work of Aijun Song was supported by the U.S. National Science Foundation under Grant CNS-1801861. This paper was presented in part at the International Conference on Underwater Networks & Systems, Atlanta, GA, USA, October 23–25, 2019. (Corresponding author: Miao Pan.)

Associate Editor: C.Tsimenidis.

Debing Wei, Chaoxian Qi, Chenpei Huang, Jiefu Chen, and Miao Pan are with the Department of Electrical and Computer Engineering, University of Houston, Houston, TX 77204 USA (e-mail: dwei3@uh.edu; cqi4@uh.edu; chuang30@uh.edu; jchen84@uh.edu; mpan2@uh.edu).

Aijun Song is with the Department of Electrical and Computer Engineering, University of Alabama, Tuscaloosa, AL 35487 USA (e-mail: song@eng.ua.edu). Gangbing Song is with the Department of Mechanical Engineering, University of Houston, Houston, TX 77204 USA (e-mail: gsong@uh.edu).

Digital Object Identifier 10.1109/JOE.2021.3085098

Index Terms—Pipeline, stress wave, subsea environment, wireless communication.

I. INTRODUCTION

FFSHORE pipeline is considered to be the most efficient and effective modes of transport for carbon products. Owing to the escalating demand for oil and gas, thousands of miles of offshore pipelines have been deployed all over the world. Taking the Gulf of Mexico as an example, over 44 000 miles of pipelines have been deployed during the last century [1]. The State of the Coast website boasts of the U.S. National Oceanic and Atmospheric Administration (NOAA), "if placed end to end, the oil and gas pipelines in the Gulf of Mexico could wrap around the earth's equator." The lifespan of the offshore pipeline is around 40 years. By far, a large portion of offshore pipelines is out of service. For example, there are more than 18 000 miles of "out-of-service" pipelines in the Gulf of Mexico [1]. However, all these offshore pipelines can be potentially utilized as a propagation medium and apply stress wave waveguide technology for subsea data transmissions [2], [3].

In comparison with acoustic wireless communications, stress wave communications (SWC) have many advantages. First, the propagation velocity of stress wave along a steel pipe can be more than 5500 m/s, which is over three times faster than the speed of acoustic waves. Hence, smaller communication delay can be expected. Second, the acoustic wave suffers from geometric spreading loss since the sound energy is radiated equally in all directions. On the contrary, the propagation of the stress wave is only along one dimension, so that no geometric spreading loss needs to be concerned. Thus, the power consumption for SWC can be much smaller than acoustic communications. Third, unlike the acoustic channel, which is strongly affected by the surrounding environments, e.g., pressure and temperature, the stress wave channel is much more stable and robust. This is because once the transmitter and receiver were located on the pipe, the stress wave channel condition would be deterministic. Therefore, highly reliable data transmissions can be realized through SWC with small bit error rate.

Compared to electromagnetic (EM)-based underwater wireless communications, the advantages for SWC are also obvious. Due to the high conductivity of seawater, the propagation of high-frequency (over megahertz) EM waves suffers from severe attenuation. As a consequence, only the low-frequency quasi-static magnetic fields can be utilized for data transmission, which is referred to as underwater magnetic induction (MI)

1558-1691 © 2021 IEEE. Personal use is permitted, but republication/redistribution requires IEEE permission. See https://www.ieee.org/publications/rights/index.html for more information.

wireless communications [4]–[7]. Both the theoretical studies and field tests [8] suggest that the practical subsea communication range of MI wireless communications is within 1 or 2 m. The attenuation of stress wave along a steel pipe is surprising low [9], approximately few decibel per thousand feet. Hence, the communication range is determined by the length of the pipeline network, which can be potentially up to kilometers.

This article attempts to investigate the SWC along offshore pipelines, whereas a couple of researchers have demonstrated SWC on some other solid mediums with different titles of this technology. Johnson [10] had demonstrated seismic communications with a data rate of 2 pulses/s at a distance of 760 ft through hard rocks back in 1972. Lawry et al. [11] present a system capable of high data rate transmission through solid metal barriers using ultrasound. The proposed prototype has realized 12.4-Mb/s transmission data rate by using the orthogonal frequency-division multiplexing (OFDM) modulation scheme. But the communication media of their system is a 2-in metal wall, which is completely different from a long pipe. Siu et al. investigate a specific concrete channel model for SWCs in [12] and [13]. The impulse response for a 60-in concrete channel is tested by experiments. The maximum data rate that can be achieved by this specific channel is also evaluated based on experiment results. Ji et al. investigated the time-reversalbased pulse position modulation for SWC in concrete structures in [14]. Unfortunately, no general channel model for SWC can be found in these works. There are several key challenges need to be tackled for SWC, which include: 1) the path loss model of stress wave propagating through a pipeline; 2) the available bandwidth; and 3) dispersion proprieties and channel response.

In this article, we carefully study the unique features of stress wave channel along a hollow cylindrical pipe. In particular, based on the governing equations, we analyze the dispersion of stress wave, which will cause the unique multimode propagation. Furthermore, we propose a attenuation model to study the path loss and frequency selective channel response. We also build up a SWC testbed and evaluate the communication performance both in the air and in the seawater. Our salient contributions are summarized as follows.

- 1) We detailed analyzed the propagation of the stress wave along a hollow pipe. The mode analysis allowed us to find a specific frequency range that is most suitable for SWCs.
- 2) We investigate the multimode propagation propriety caused by the dispersion of stress waves, which introduces significant intersymbol interference (ISI).
- 3) We derived the attenuation of L(0,2) and T(0,1) modes, which are two ideal modes that can be utilized for SWCs. Furthermore, we estimate the channel path loss and the frequency selective channel response.
- 4) We set up a SWC testbed. A series of experiments were carried out to measure the stress wave channel response including impulse response and frequency responses. We also evaluate the SWC performances in the seawater as well as in the air.

The rest of this article is organized as follows. We summarize the related work in Section II. Section III gives the theoretical analysis to the propagation of stress wave. Section IV

investigates the stress wave channel characteristic. In Section V, we demonstrate our experiment platform, and evaluate the performance of the SWC along a steel pipe both in the air and underwater. We conclude this article and point to directions for future work in Section VI.

II. RELATED WORK

Stress wave has been commonly used for nondestructive testing (NDT) and structure health monitoring (SHM) [15], [16] since 1940. The propagation characteristics of stress wave along buried pipelines have been presented in [17]. The fundamental principle for NDT is analyzing the echo of impulse signal to detect the location of structure defects, e.g., cracks, which is different from communication technologies.

As early as 1972, Johnson [10] had demonstrated seismic communications at a distance of 760 ft through hard rocks with a data rate of 2 pulse/s. In comparison to RF wireless communications, such a poor-communication performances make it barely useful in the area where RF technology is applicable.

The similar communication approach had been applied to the high-rate acoustic logging while drilling (LWD) telemetry through drill-strings since 1948. The propagation analysis of acoustic waves along drill-strings can be found in [9] back in 1989. It was concluded that the attenuation is surprisingly low, less than 4 dB/1000 ft; and the difficultly is suppressing the echo and background noise. The drill-string channel consists of pipes and joints periodically, which results in a comb-filteringlike channel transfer functions. The corresponding channel capacity of an LWD acoustic telemetry system under drilling conditions is calculated in [18], which concludes that the practical data rate is around 500 b/s for the 6000-ft drill-string channel. The adaptive OFDM is regarded as the promising modulation scheme for such comb-filteringlike channels as shown in [19]-[21]. The most significant different between pipeline channel and drill-string channel is that the pipeline is well welded during the deployment. Hence, more flat channel transfer function would be expected for pipeline channels. Furthermore, the background noise for pipeline channels is much lower than drill-string channels. Therefore, much better communication performances could be expected for a pipeline SWC system compared with a drill-string LWD acoustic telemetry system.

In recent years, wireless sensor networks (WSNs) are considered to be a compelling platform for SHM [22], [23]. Since concrete structures are usually planted underground or immersed underwater, the signal is shielded by the environment and it is not realizable to use the long-distance radio communication. Therefore, SWC may find its applications in WSN for SHM. In 2012, Kailaswar *et al.* propose ConcreteComm using stress wave and successfully demonstrate a 10-kb/s wireless link on a concrete block with dimension of $60 \times 12.5 \times 8''$ [24]. Later, Siu *et al.* investigate the impulse response of the concrete channel and channel capacity of SWC for a 60-in concrete channel in [12].

The acoustic signal is currently the only physical signal that can be used as the carrier for long-range (up to kilometers) underwater wireless communications. Since the 1990s, a large

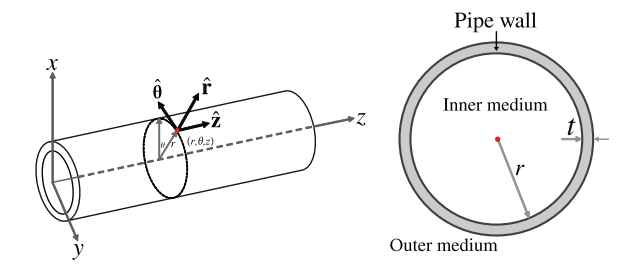


Fig. 1. Hollow acoustic waveguide in cylindrical coordinate and its cross section.

number of efforts have been pursued in the area of underwater acoustic communications. The underwater acoustic communication data rate has been improved through spectral efficient modulation schemes, spatial diversity, and high-performance equalizers [25]. However, the available bandwidth of underwater acoustic channels is seriously limited since the propagation loss of acoustic wave in the water is quite frequency selective [26], [27]. Furthermore, the communication performance can be seriously affected by the surrounding environments. For example, the acoustic links can be easily damaged by the temperature gradients of the seawater, Doppler effect, surface ambient noise and multipath propagation due to reflection and refraction [28], [29]. On the contrary, the channel conditions of stress wave are much more stable than the acoustic waves, since the propagation path of stress wave is guided along the pipeline, which can be consider as a time-invariant consistent channel. We have shown some sea test results in [30]. However, in this article, the theoretical analysis of stress wave channel characteristics including path loss, fading proprieties, and channel responses are detailed.

III. STRESS WAVE PROPAGATION ANALYSIS

In this section, the displacement field of a hollow cylindrical pipe is first investigated. Then, the dispersion relation of the stress wave is analyzed. Finally, the attenuation of two favorite modes, L(0,2) and T(0,1), were formulated.

A. Displacement Field Analysis

Many industrial pipelines such as oil and gas pipeline systems and urban water distribution networks are buried underground, underwater, and are mostly isolated and inaccessible. The stress wave channel considered in this article consists of an inner fluid medium, a solid cylindrical waveguide (pipe wall), and an outer fluid medium, as shown in Fig. 1.

The stress wave propagation in an elastic or viscoelastic medium is governed by Navier's equation, which is in the form of

$$\mu \nabla^2 \mathbf{u} + (\lambda + \mu) \nabla (\nabla \cdot \mathbf{u}) = \rho \left(\frac{\partial^2 \mathbf{u}}{\partial t^2} \right)$$
 (1)

where λ and μ are Lamé constants, which determine the bulk wave velocity of the material. \mathbf{u} is the displacement vector and ρ is the material density. To simplify this problem, Helmholtz's

decomposition is applied to the displacement vector in (1). The displacement vector then is decomposed by a combination of the scalar potential, Φ , and vector potential, Ψ , as

$$\mathbf{u} = \nabla \Phi + \nabla \times \mathbf{\Psi}.\tag{2}$$

Substituting (2) into (1) and using calculus identities for simple algebra, (1) can be decomposed into two equations as follows:

$$\left(\frac{\partial^2 \Phi}{\partial t^2}\right) - \left(\frac{\lambda + 2\mu}{\rho}\right) \nabla^2 \Phi = 0 \tag{3}$$

and

$$\left(\frac{\partial^2 \mathbf{\Psi}}{\partial t^2}\right) - \left(\frac{\mu}{\rho}\right) \nabla^2 \mathbf{\Psi} = 0. \tag{4}$$

Equations (3) and (4) fall into the scalar Helmholtz equation and vector Helmholtz equation, respectively. Two additional constants c_l and c_s are defined as

$$\begin{cases} c_l = \sqrt{\frac{\lambda + 2\mu}{\rho}} \\ c_s = \sqrt{\frac{\mu}{\rho}} \end{cases}$$
 (5)

where c_l denotes the longitudinal bulk wave velocity and c_s is the shear bulk wave velocity. With the assumption that the hollow cylinder is elastic isotropic and infinity long, the boundary condition at two ends can be ignored. On the inner and outer surfaces of the pipe, the traction-free boundary condition is considered.

In cylindrical coordinate, the Laplacian terms in (3) and (4)

$$\begin{cases}
\nabla^{2}\Phi = \frac{\partial^{2}\Phi}{\partial r^{2}} + \frac{1}{r}\frac{\partial\Phi}{\partial r} + \frac{1}{r^{2}}\frac{\partial^{2}\Phi}{\partial\theta^{2}} + \frac{\partial^{2}\Phi}{\partial z^{2}} \\
\nabla^{2}\Psi = \left(\nabla^{2}\Psi_{r} - \frac{1}{r^{2}}\Psi_{r} - 2\frac{1}{r^{2}}\frac{\partial\Psi_{\theta}}{\partial\theta}\right)\hat{\boldsymbol{r}} \\
+ \left(\nabla^{2}\Psi_{\theta} - \frac{1}{r^{2}}\Psi_{\theta} - 2\frac{1}{r^{2}}\frac{\partial\Psi_{r}}{\partial\theta}\right)\hat{\boldsymbol{\theta}} + \nabla^{2}\Psi_{z}\hat{\boldsymbol{z}}.
\end{cases} (6)$$

Combining (3), (4), and (6), Rose *et al.* presented the solutions for the scalar and vector potentials in [31] as

$$\begin{cases}
\Phi = f(r)e^{im\theta}e^{i(kz-\omega t)} \\
\Psi_r = \psi_r(r)e^{im\theta}e^{i(kz-\omega t)}, \quad m = 0, 1, 2... \\
\Psi_\theta = \psi_\theta(r)e^{im\theta}e^{i(kz-\omega t)} \\
\Psi_z = \psi_z(r)e^{im\theta}e^{i(kz-\omega t)}
\end{cases} (7)$$

where the integer m is known as the circumferential order of a wave mode and k is the wave number. f, ψ_r , ψ_θ and ψ_z are Bessel functions as shown in Appendix A.

B. Dispersion Analysis

In a waveguide such as a pipe, partial bulk wave reverberates between boundaries along the pipe. There are a bunch of waveforms with different propagation characteristics, which are known as "modes." For pipe geometry, stress waves are generally divided into three groups, namely the torsional (T), longitudinal (L), and flexural (F) waves. These modes are labeled as L(0, m), T(0, m), and F(n, m), where n and m are integers. The number of modes increases as the operating frequency is exceeding the cutoff frequency, which is the lowest frequency

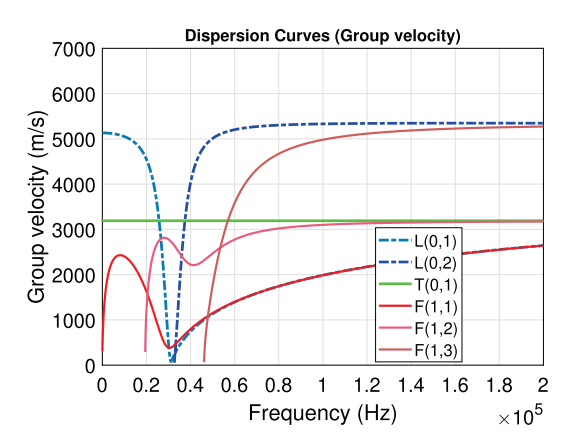


Fig. 2. Group velocities versus frequency. L (0, n) is the longitudinal mode, T (0, n) is the transverse mode, and F (m, n) is the flexural mode. m is the order of cyclic variation, and n is a counterindex.

for which a mode can propagate in the pipe [32]. The propagation velocity of different modes depends on frequency, which is known as dispersion. Every mode has its cutoff frequency, dispersion characteristic, and attenuation. Dispersion will cause ISI to the stress wave channel from the perspective of wireless communications.

Based on the solution of governing equation, Rose *et al.* [31] derived the phase and group velocities as

$$\begin{cases} c_p = \omega/k \\ c_g = \frac{\partial \omega}{\partial k} \end{cases}$$
 (8)

where c_p and c_q are phase and group speed, respectively. They are both the function of wave number k. To investigate the dispersion, the open-source package GUIGUW [33] is used to simulate the modes distribution. GUIGUW utilizes a semianalytical finite-element (SAFE) approach to model ultrasonic propagation in cylindrical, plate, and arbitrary cross section waveguides. Group velocities, which describe the propagating speeds of guided wave packets with components of different frequencies, are calculated by GUIGUW. They are very critical in guided wave applications as the measured velocities by transducers are usually group velocities. Group speed dispersion curves allow us to identify guided wave modes in guided wave tests. Group velocities of different modes are calculated and shown in Fig. 2. In the simulation, the inner and outer diameters of the steel hollow pipe are set to 2 and 2.12 in, respectively, so the thickness of pipe wall is 0.06 in. The density of the steel pipe is 7800 kg/m³. Young's modulus of the steel at room temperature is 200 GPa.

To simplify the interpretation of the received signals in the experiment, it is desirable to excite a single mode. Especially, in a long-range communication, it is practically essential exciting a single mode to maximize the signal-to-noise ratio (SNR) and decrease the power dissipation. The excitation of a single-mode stress wave can be achieved by using a ring transducer, more details can be found in [34] and [35].

The group velocities give us insight into the mode distribution on the frequency spectrum. Much attention should be paid to the green curve, i.e., T(0,1) mode. It indicates that the velocity is a constant in the entire frequency range. T(0,1) mode is considered as the best one as it is nondispersive, whereas T(0,1) is slower compared with L(0,n) and F(1,3) in feasible frequency ranges. In the dispersive stress-wave channel, the slow T(0,1) mode might cause significant delay spreads and hinder the high-data-rate transmissions. L(0,2) mode at a frequency between 40 and 120 kHz is an alternative one that is conducive to communication. As shown in Fig. 2, the group speed of L(0,2) from 40 to 120 kHz is almost constant, thus approximately nondispersive and the mode shape remains unchanged while propagation. Furthermore, L(0,2) is the fastest mode among those modes coexisting in the entire frequency range.

For the structure health monitoring, there exist some postprocessing algorithms that can remove the undesired propagating modes, such as narrowband filtering and time-of-flight (TOF) filtering [35], [36]. For example, as shown in Fig. 2, the spectrum around 30 kHz is the stopband of lots of modes; therefore, applying a narrowband filter around 30 kHz can pick out the T(0,1) mode. If the signal duration is short enough, the fast mode can be separated from slow mode in time domain through TOF. However, none of these algorithms are suitable for communications. Since for communications, the symbol duration cannot be very short, and the wide bandwidth is preferred for high-speed communications.

C. Attenuation Analysis

Navier's equation, as shown in (1), does not consider the energy loss. This means that the displacement field obtained from it will propagate without attenuation. Obviously, such a mathematical model is too ideal to be suitable for stress wave channel modeling.

The main reason that (1) is lossless is that it adopts lossless medium constitutive relations, which are shown as follows:

$$\begin{cases}
\sigma_{11} = (\lambda + 2\mu)\varepsilon_{11} + \lambda\varepsilon_{22} + \lambda\varepsilon_{33} \\
\sigma_{22} = \lambda\varepsilon_{11} + (\lambda + 2\mu)\varepsilon_{22} + \lambda\varepsilon_{33} \\
\sigma_{33} = \lambda\varepsilon_{11} + \lambda\varepsilon_{22} + (\lambda + 2\mu)\varepsilon_{33} \\
\sigma_{23} = 2\mu\varepsilon_{23} \\
\sigma_{31} = 2\mu\varepsilon_{31} \\
\sigma_{12} = 2\mu\varepsilon_{12}
\end{cases} \tag{9}$$

where σ_{ij} is the stress tensor, ε_{ij} is the strain field, and i, j indicate different dimensions in different coordinate systems.

To model the attenuation of stress wave propagation, we need to modify (9). One way is by adding a viscous damping term. For example, we change

$$\sigma_{12} = 2\mu\varepsilon_{12}$$

to

$$\sigma_{12} = 2\mu\varepsilon_{12} + \eta_{12}\frac{\partial\varepsilon_{12}}{\partial t}$$

where η_{ij} is the viscosity constant.

From the dispersion curves Fig. 2, we can see that mode T(0,1) does not have dispersion, and mode L(0,2) barely has dispersion when the frequency is over 60 kHz. Therefore, they are two

potential modes that can be utilized for SWCs. Correspondingly, we will focus on the attenuation analysis of these two modes.

1) Attenuation of L(0,2) Mode: Since longitudinal modes do not have tangential displacement component, we can assume that the displacement fields take the form as

$$\begin{cases} u_r = f(r)e^{i(kz-\omega t)} \\ u_\theta = 0 \\ u_z = ig(r)e^{i(kz-\omega t)}. \end{cases}$$
 (10)

The corresponding strain and stress fields are as follows:

$$\begin{cases} \varepsilon_{rr} = f'e^{i(kz-\omega t)} \\ \varepsilon_{\theta\theta} = \frac{1}{r}fe^{i(kz-\omega t)} \\ \varepsilon_{zz} = -kge^{i(kz-\omega t)} \\ \varepsilon_{\theta z} = 0 \\ \varepsilon_{zr} = \frac{1}{2}i(kf + g')e^{i(kz-\omega t)} \\ \varepsilon_{r\theta} = 0 \end{cases}$$

$$(11)$$

and

$$\begin{cases}
\sigma_{rr} = \left[(2\mu + \lambda)f' + \lambda(\frac{1}{r}f - kg) \right] e^{i(kz - \omega t)} \\
\sigma_{\theta\theta} = \left[(2\mu + \lambda)\frac{1}{r}f + \lambda(f' - kg) \right] e^{i(kz - \omega t)} \\
\sigma_{zz} = \left[-(2\mu + \lambda)kg + \lambda(f' + \frac{1}{r}f) \right] e^{i(kz - \omega t)} \\
\sigma_{\theta z} = 0 \\
\sigma_{zr} = i\mu(kf + g')e^{i(kz - \omega t)} \\
\sigma_{r\theta} = 0.
\end{cases} (12)$$

According to the equilibrium equation

$$\nabla \cdot \boldsymbol{\sigma} = \rho \frac{\partial^2 u}{\partial t^2}$$

we have the following:

$$g'' + \frac{1}{r}g' + \frac{\rho\omega^2 - (2\mu + \lambda)k^2}{\mu}g + \frac{k(\mu + \lambda)}{\mu}\left(f' + \frac{1}{r}f\right) = 0$$
(13)

and

$$f'' + \frac{1}{r}f' - \frac{1}{r^2}f + \frac{\rho\omega^2 - \mu k^2}{\lambda + 2\mu}f - \frac{k(\lambda + \mu)}{\lambda + 2\mu}g' = 0.$$
 (14)

The solution to (13) and (14) yields

$$\begin{cases}
f(r) = F_1 r + F_2 \frac{1}{r} \\
g(r) = G \\
\rho \omega^2 - \mu k^2 = 0 \\
kG = 2F_1
\end{cases}$$
(15)

where F_1, F_2 , and G are three constants.

Substituting μ with $\mu - i\omega\eta$, and k with $k + i\alpha$ in $\rho\omega^2 - \mu k^2 = 0$ yields

$$\mu(k^2 - \alpha^2) + 2\alpha k\omega \eta = \rho \omega^2 \tag{16}$$

and

$$i((k^2 - \alpha^2)\omega\eta - 2\alpha k\mu) = 0.$$
(17)

By solving (16) and (17), we can obtain the attenuation factor α as

$$\alpha^{2} = \frac{\rho \omega^{2}}{2\mu} \left(\sqrt{\frac{\mu^{2}}{\mu^{2} + \omega^{2} \eta^{2}}} - \frac{\mu^{2}}{\mu^{2} + \omega^{2} \eta^{2}} \right). \tag{18}$$

Considering $\mu \gg \omega \eta$, expression (18) reduces to

$$\alpha = \frac{\omega^2 \eta}{2\mu} \sqrt{\frac{\rho}{\mu}}.$$
 (19)

2) Attenuation of T(0,1) Mode: The T(0,1) mode only has the tangential displacement component. Therefore, the displacement fields would be

$$\begin{cases}
 u_r = 0 \\
 u_\theta = h(r)e^{i(kz - \omega t)} \\
 u_z = 0.
\end{cases}$$
(20)

Following the similar procedure as in previous section, we have

$$\mu \left(h'' + \frac{1}{r}h' - \frac{1}{r^2}h - k^2 h \right) = -\rho \omega^2 h. \tag{21}$$

Substituting μ with $\mu - i\omega\eta$, and k with $k + i\alpha$, where α is the attenuation factor, yields

$$\mu \left[h'' + \frac{1}{r}h' - \frac{1}{r^2}h - (k^2 - \alpha^2)h \right] - 2\alpha k\omega \eta h + \rho \omega^2 h$$
$$-i \left\{ \omega \eta \left[h'' + \frac{1}{r}h' - \frac{1}{r^2}h - (k^2 - \alpha^2)h \right] + 2\alpha k\mu h \right\} = 0. \tag{22}$$

The solution to (22) is

$$h(r) = AZ_1(\beta r) + BW_1(\beta r) \tag{23}$$

where

$$\beta = \sqrt{\frac{\mu\rho\omega^2}{\omega^2\eta^2 + \mu^2} - (k^2 - \alpha^2)}$$

and Z_1 and W_1 are the first-order Bessel functions. The boundary conditions are $\sigma_{r\theta} = 0$ at r = a and r = b, where a, b are the inner and outer radii of the pipe, respectively. Since

$$\sigma_{r\theta} = \mu(h' + \frac{1}{r}h)e^{i(kz - \omega t)}$$

we have

$$\begin{bmatrix} Z_1'(\beta a) - \frac{Z_1(\beta a)}{a} & W_1'(\beta a) - \frac{W_1(\beta a)}{a} \\ Z_1'(\beta b) - \frac{Z_1(\beta b)}{b} & W_1'(\beta b) - \frac{W_1(\beta b)}{b} \end{bmatrix} \begin{bmatrix} A \\ B \end{bmatrix} = 0.$$
 (24)

By solving (24), we can obtain β . Finally, we can solve the wave number k, and attenuation factor α by solving

$$k^{2} - \alpha^{2} = \frac{\mu\rho\omega^{2}}{\omega^{2}n^{2} + \mu^{2}} - \beta^{2}$$
 (25)

and

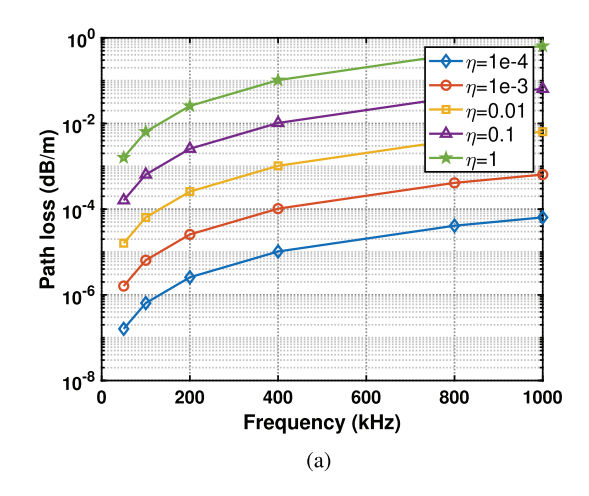
$$2\alpha k = \frac{\eta \rho \omega^3}{\omega^2 \eta^2 + \mu^2}. (26)$$

By eliminating k from (25) and (26), we obtain

$$2\alpha^2 = \frac{1}{2} \frac{(\eta \rho \omega^3)^2}{(\mu^2 + \eta^2 \omega^2)(\mu \rho \omega^2 - \beta^2(\mu^2 + \eta^2 \omega^2))}.$$
 (27)

Considering $\rho\omega^2\gg\mu\gg\omega\eta$ and $\beta\approx 1$, expression (27) reduces to

$$\alpha = \frac{\omega^2 \eta}{2\mu} \sqrt{\frac{\rho}{\mu}}.$$
 (28)



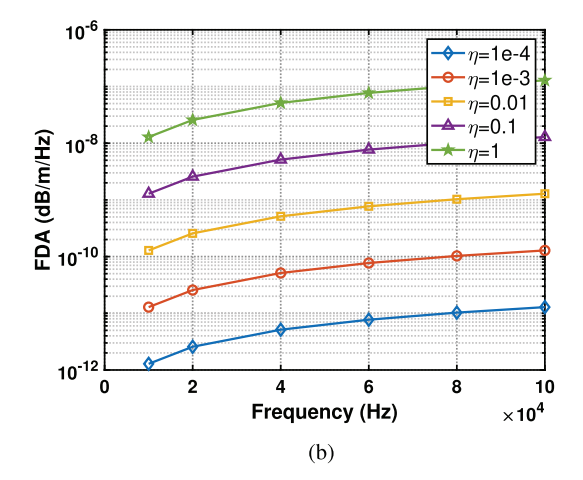


Fig. 3. (a) Path loss and (b) frequency-dependent attenuation of the stress wave channel.

The comparison between (19) and (28) reveals that longitudinal modes and torsional modes share the same attenuation rate, which is proportional to the square of the frequency.

IV. STRESS WAVE CHANNEL CHARACTERISTICS

In this section, we will first investigate the path loss of the stress wave channel. Then, the unique multimode dispersion is analyzed. Finally, the multipath channel response is evaluated.

A. Path Loss

Based on the attenuation analysis in Section III, we can estimate the path loss of the stress wave channel. The attenuation of displacement fields between two points with different z coordinates z_1 and z_2 ($z_2 > z_1$) is $e^{-\alpha(z_1-z_2)}$. Hence, the path loss can be calculated as

pathloss (dB/m) =
$$20(\log e)\alpha \approx 8.686\alpha$$
. (29)

Combining (28) and (29), we can evaluate the path loss of the stress wave channel. The typical value of shear modular μ of steels is in the order of 10, e.g., 8.24×10^{10} N/m². β is approximately equal to 1, which is determined by the inner and outer radius of the pipe. The density of stainless steel is around 7850 kg/m³. The only uncertain parameter in (28) is the viscosity constant used to model the propagation loss of stress wave. Suppose η is around 1, then the path loss of stress wave is approximately equal to 0.006 dB/m if the operation frequency is 100 kHz.

We can also estimate the frequency-dependent attenuation (FDA) characteristics based on (28). The attenuation between two frequencies f_1 and f_2 ($f_2 > f_1$) can be calculated by $e^{-\gamma(f_1-f_2)}$, where

$$\gamma = 4\pi^2 d\frac{\eta}{\mu} \sqrt{\frac{\rho}{\mu}} f_c$$

d is the transmission distance, and

$$f_c = \frac{f_2 + f_1}{2}$$

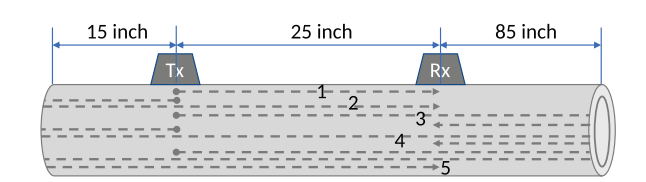


Fig. 4. Reflections of the stress wave along a pipe.

is the carrier frequency. Similarly, the FDA can be estimated as

FDA (dB/Hz) =
$$20(\log e)\gamma \approx 8.686\gamma$$
. (30)

The path loss and FDA curves of the stress wave channel are plotted in Fig. 3. Generally speaking, the viscosity constant of metals is a small number, $\eta \ll 1$. Therefore, the propagation loss of the stress wave along a hollow cylindrical pipe would be extremely small. From this point of view, the stress wave channel of a pipe with infinite length can be regarded as a flat fading channel if the operation frequency is under megahertz level.

B. Multimode Dispersion

As shown in Fig. 2, the propagation of stress wave in a pipe exhibits different modes. Moreover, different modes propagate in different speeds. As a consequence, the delay spread of the stress wave channel is distance related. For example, according to Fig. 2, suppose the transmitted symbol was dominated by L(0,2) and T(0,1) mode, the delay spread caused by multimode propagation can be estimated as

$$\tau = \frac{d}{v_T} - \frac{d}{v_L} \tag{31}$$

where d is the distance between the transmitter and receiver, v_L and v_T are the propagation velocity of L(0,2) mode and T(0,1) mode, respectively. As shown in Fig. 2, $v_L \approx 5000$ m/s and $v_T \approx 3000$ m/s, so the delay spread for d=100 m is around 13.3 ms. Such a huge delay spread implies that the symbol rate of SWC must be slow to avoid the ISI.



Fig. 5. Received symbol determination process.

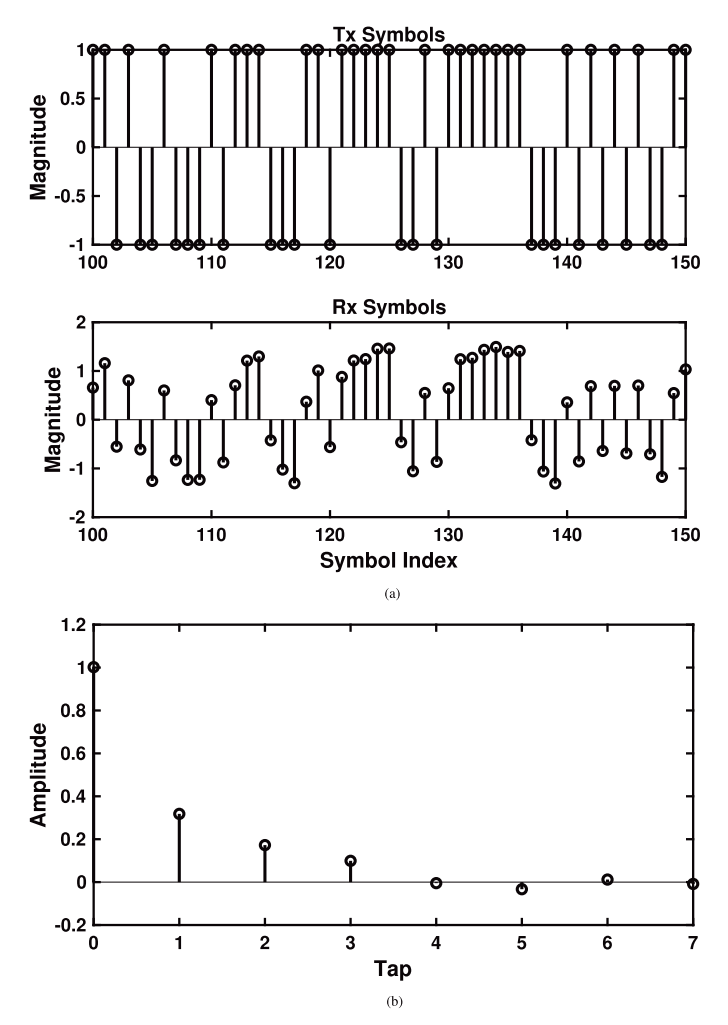


Fig. 6. Channel response of the stress wave channel. (a) Transmitted and received symbols. (b) Channel response.

C. Multipath

The propagation of stress wave along a pipe will suffer from strong echos, which are the reflections from both ends of the pipe. As shown in Fig. 4, the propagation delay of each reflection path can be determined by the length of the pipe and the positions of the transmitter and receiver. If we only consider the first reflection from both ends, path 5 would be the longest path, which is 265 in. Since the propagation speed of T(0,1) mode is 3.2 km/s, the propagation delay would be 2.1 ms.

The channel response can be estimated by transmitting pilot symbols denoted as $\mathbf{t}[n]$. Suppose the channel impulse response is denoted as $\mathbf{h}[m]$. Then, the received symbols denoted as $\mathbf{r}[n]$ can be expressed as

$$\mathbf{r} = \mathbf{t} * \mathbf{h}. \tag{32}$$

The matrix form of (32) is

$$\mathbf{r} = \mathbf{Th} \tag{33}$$

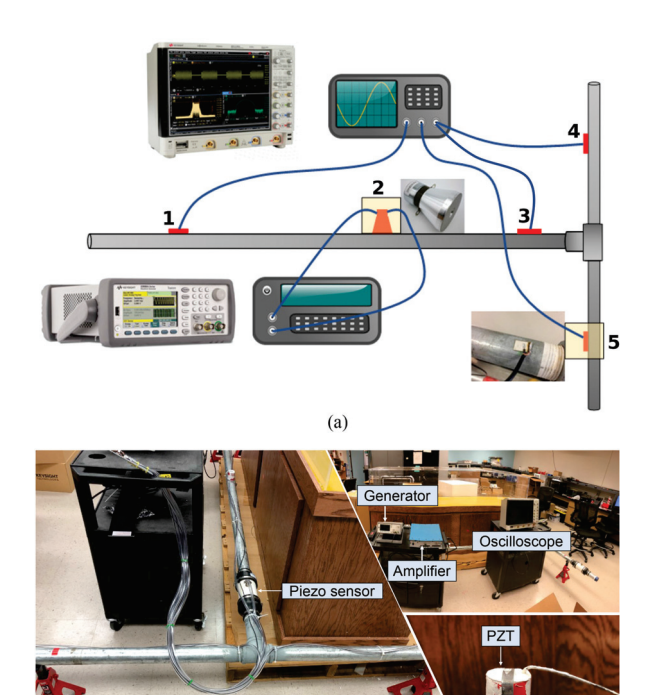


Fig. 7. Lab testbed of SWC. (a) Schematic of the testbed. (b) Lab testbed.

(b)

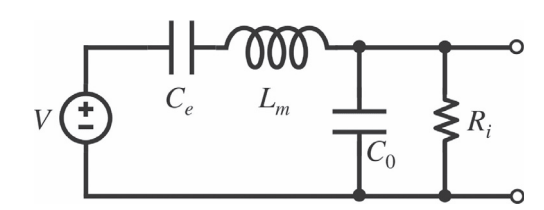


Fig. 8. Equivalent circuit model of piezoelectric transducer.

where T is the transmission matrix as

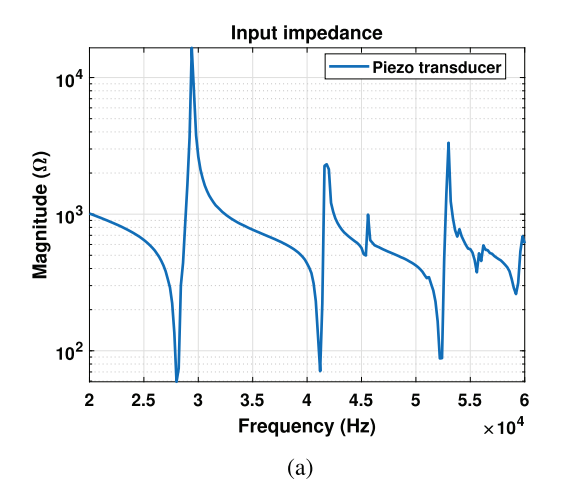
$$\mathbf{T} = \begin{bmatrix} \mathbf{t}[\mathbf{0}] & \mathbf{t}[-1] & \cdots & \mathbf{t}[1-m] \\ \mathbf{t}[1] & \mathbf{t}[0] & \cdots & \mathbf{t}[2-m] \\ \vdots & \vdots & \vdots & \vdots \\ \mathbf{t}[n-1] & \mathbf{t}[n-2] & \cdots & \mathbf{t}[n-m] \end{bmatrix}. \tag{34}$$

The number of transmitted pilot symbols n is normally much larger than the number of taps of channel impulse response m. Therefore, we can apply least square method to solve (33) and the solution is

$$\mathbf{h} = (\mathbf{T}^\mathsf{T}\mathbf{T})^{-1}\mathbf{T}^\mathsf{T}\mathbf{r}.\tag{35}$$

In our experiments, the pilot symbols were modulated by BPSK, the amplitude of which is either 1 or -1. Before we apply (35), we need to obtain the received symbol vector \mathbf{r} . The corresponding signal processing process is shown as in Fig. 5.

The transmitted symbols and the corresponding received symbols are shown in Fig. 6(a). The symbol rate of the experiment is 1 kBd (1000 sps), which means the symbol period is 1 ms. According to our previous analysis, the propagation delay is



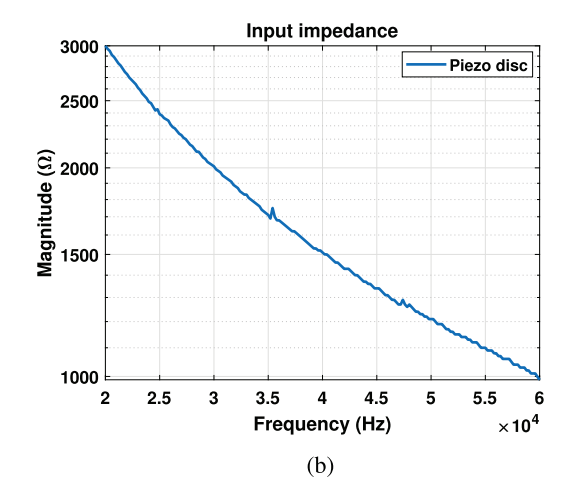


Fig. 9. Input impedance of piezoelectric elements. (a) PZT stack. (b) PZT disc.

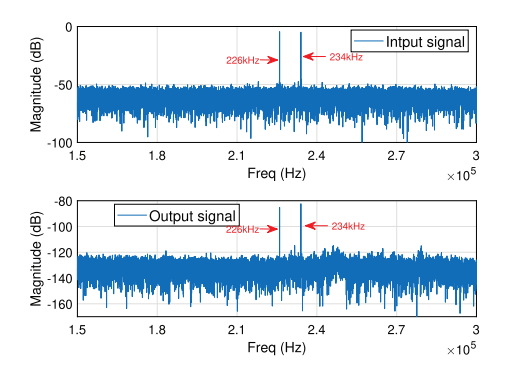


Fig. 10. Absolute value of the Fourier transform of the amplitude when transmitting two sinusoidal signals simultaneously at 226 kHz and 234 kHz, respectively.

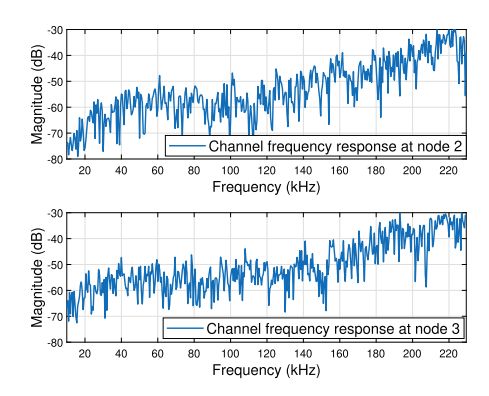


Fig. 11. Frequency responses of the stress wave testbed.

around 2.1 ms, which implies that the current symbol may be contaminated by its previous three symbols. Therefore, the channel response can be expected as a four tap FIR filter, which is verified by the experiment result, as shown in Fig. 6(b). Although we use seven tap FIR filter to model the channel response, only the first four taps have significant magnitude. Hence, Fig. 6(b) implies that the length of the channel response should be between 2 and 3 ms.

V. EXPERIMENT EVALUATION

Although the theoretical analysis suggests that the single-mode stress wave channel of an infinite-length pipe can be treated as a flat fading channel, a finite-length pipe will suffer from strong distortion caused by the reflection from both ends as well as multimode dispersion. Moreover, the frequency response of the piezoelectric transducer is also frequency selective. Therefore, the practical stress wave channel would be much more complicated. In this section, we will first set up a stress wave testbed. Then, we will measure the practical stress wave channel response. Finally, we will evaluate the practical SWC performances.

A. SWC Testbed

The testbed is built on two galvanized steel pipes with length of 10 ft and diameter of 2 in. The pipes are weld together to form a "T" shape, such that we can investigate the reflection when the stress wave propagates through a joint. The piezoelectric transducer was applied on the surface of the pipe for the conversion between electric signals and mechanical vibrations. The transmitted signal is generated by a signal generator (Keysight 33500B) while the received signal is captured and recorded by a oscilloscope (Keysight MSOS604). The schematics of the testbed and real testbed are shown in Fig. 7. Before we can apply any wireless communion schemes, we need to figure out the available bandwidth of the aforementioned testbed. We will first design an appropriate OFDM training symbol sequence to estimate the frequency response. Then, we will evaluate the real SWC performances both in the air and in the underwater environments.

B. Transducer Characteristics

PZT, or lead zirconate titanate, is one of the world's most widely used piezoelectric ceramic materials. PZTs have strong piezoelectric effect, which is the ability to generate electric charge in response to applied mechanical stress. Therefore, the PZT transducer has been widely used as an stress wave actuator

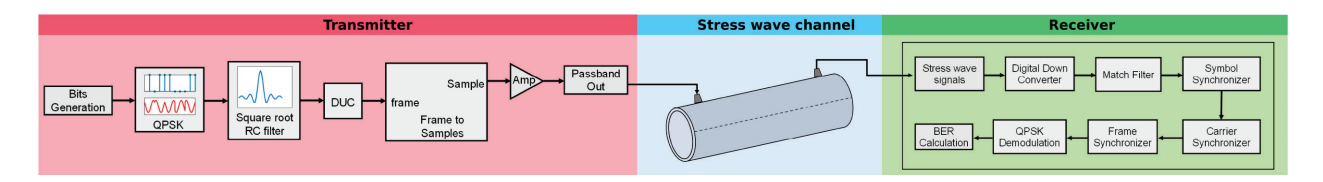


Fig. 12. Block diagram of the stress wireless communication system.

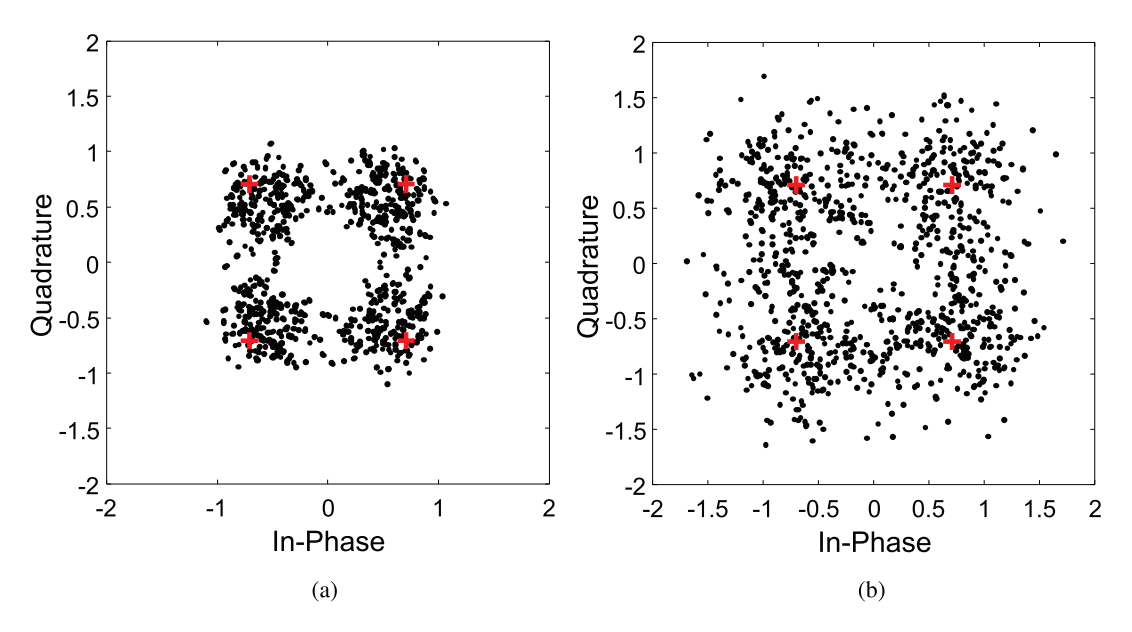


Fig. 13. Demodulation results in the lab. (a) Demodulation results at node 3, BER=0.0783 @ symbol rate = 1380. (b) Demodulation results at node 4, BER=0.2366 @ symbol rate = 1380.

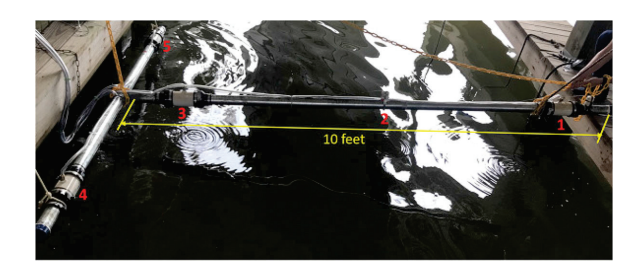


Fig. 14. Subsea testing setup.

or sensor in the field of structure health monitoring [37]–[40]. In this article, we also use PZT transducers to generate and detect stress waves. There are two different types of the PZT transducer used in our testbed, as shown in Fig. 7. Node 5 shows a single patch PZT transducer. Node 2 shows a PZT stack with multiple layer of PZT materials, which have much higher output power capability in comparison with the single PZT patch. Actually, the system operation frequency and the available bandwidth are highly related to the frequency response of the PZT transducer.

Carazo *et al.* discussed the piezoelectric transducer in detail in [41]. A equivalent circuit model, including the effects of the sensor's mechanical construction and other nonidealities,

is shown in Fig. 8. The inductance L_m is due to the seismic mass of the sensor itself. C_e is inversely proportional to the mechanical elasticity of the piezomaterial. C_0 denotes the static capacitance of the transducer, resulting from stack structure. R_i is the input resistance of the transducer element. By tuning L_m , C_e , C_0 , and impedance matching, the resonance can be established and, thus, maximize the energy transfer efficiency. The resonant equivalent circuit of the PZT sensor implies that the frequency response would be frequency selective. The input impedance of the transducer is measured as shown in Fig. 9. In Fig. 9(a), multiple peaks are observed, whereas Fig. 9(b) is smooth with no peak present. The smaller impedance means the higher energy transfer efficiency.

C. Frequency Response of the Testbed

We first experiment to verify the linear time-invariant (LTI) property of the system. In this experiment, we transmit two tones at different center frequencies simultaneously from the transmitter PZT. An oscilloscope has been utilized to record and analyze the signal from the receiver PZT. Subsequently, We perform FFT amplitude analysis. The result is shown in Fig. 10. From Fig. 10, the frequency of the received signal, which is converted from stress wave generated by transducer PZT, is the same as the input. In addition, PZT transducers

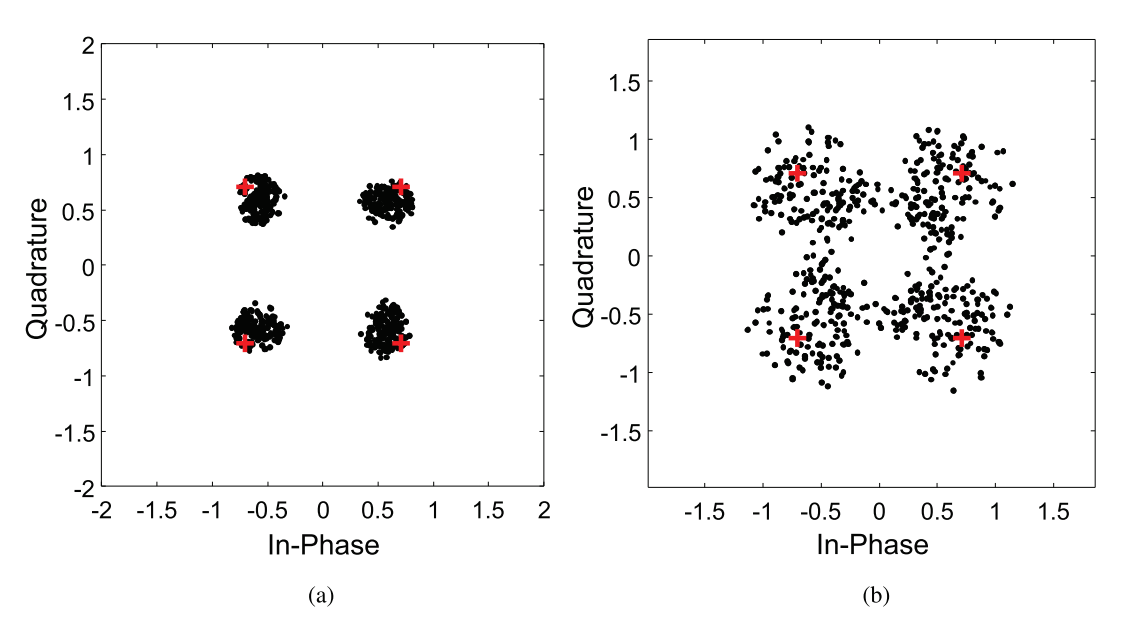


Fig. 15. Demodulation results subsea. (a) Demodulation results on node 3, BER=0 @ symbol rate = 1380. (b) Demodulation results on node 4, BER=0.1127 @ symbol rate = 1380.

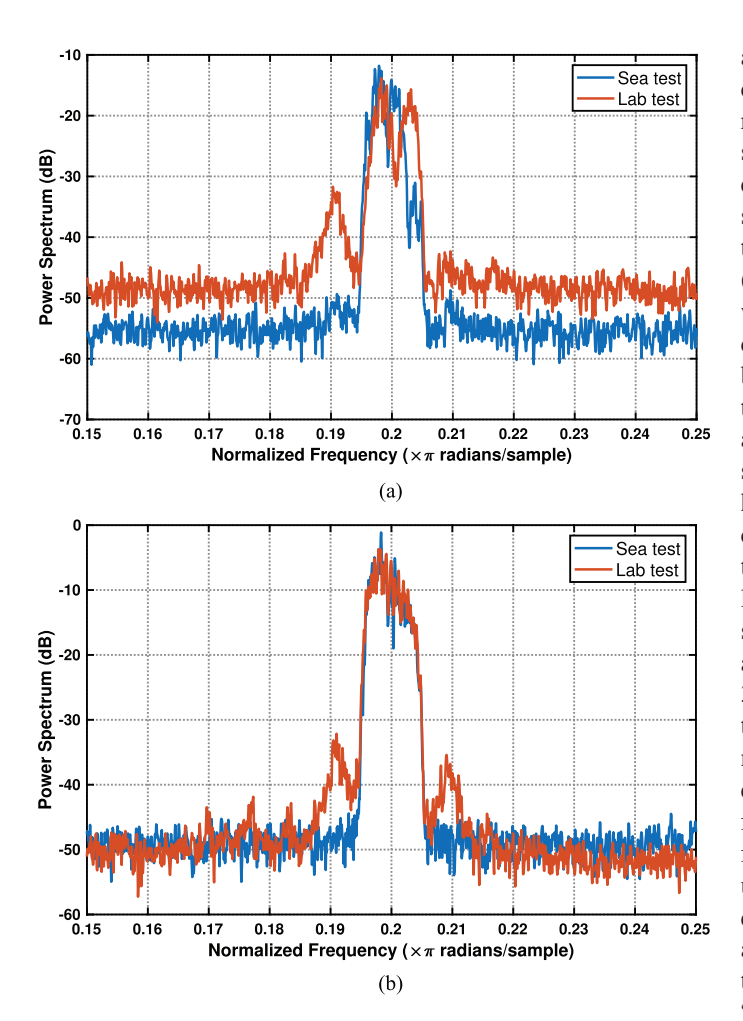


Fig. 16. Power spectrum of the received signal at nodes 3 and 4. (a) Node 4. (b) Node 3.

along with stress wave propagation over the pipeline are a linear channel since it follows scaling and additivity properties. As a result, such a linear channel enables various linear modulation schemes (BPSK, QPSK, QAM, OFDM, etc.). A channel frequency response (CFR) estimator based on the OFDM training symbol has been developed to estimate frequency response using the basic least square algorithm. The formula is the same as (33). However, in this case, the matrix T is a diagonal matrix, whose every diagonal element is a modulated symbol for its corresponding subcarrier. We investigate the stress wave channel by transmitting OFDM symbols, whose duration is 10 ms, and the sampling rate is 1 MHz. Notice that these OFDM parameters are specially designed to test the stress wave channel properties, so we adopt the narrow subcarrier spacing of 100 Hz to obtain the high-frequency resolution to precisely reflect the real stress wave channel. The cyclic prefix (CP), as the guard interval, is expected to compensate for the delay spread. In this case, we set the CP length to be 2 ms based on the fact that the theoretical delay spread is 2.1 ms. The experimental channel impulse response also suggests that the delay spread should be between 2 and 3 ms. In addition, we apply the robust QPSK modulation scheme to each subcarrier, which can tolerate a significant amount of noise (normally 12 dB SNR for 0.1% BER) for precise channel estimation. Using the parameters above, we finally show the frequency response in Fig. 11, whose bandwidth of interest is from 10 to 230 kHz. It needs to be pointed out that, although we use a conservative (very narrow) 100-Hz subcarrier spacing to extract the channel information, large subcarrier spacing such as 500 Hz is acceptable during channel estimation and data transmission. As a result, each subcarrier channel may be less "flat" but the symbol duration and the number of fast Fourier transform will decrease.

We can derive two important conclusions from Fig. 11. First, CFR follows the trend of the frequency response of the PZT

transducer as shown in Fig. 9(b), since higher frequency has higher energy conversion efficiency. Second, the frequency responses periodically experience some peak and trough, which is mainly due to the multimode and multipath propagation of the stress wave along a finite-length pipe. Specifically, if all the reflected waves are in phase with the original wave, we will observe a peak on the amplitude frequency response curve. On the other hand, the superposition of all the reflected waves and the original wave may cancel out with each other at some positions, which results in a trough on the amplitude frequency response curve.

We transmitted some QPSK symbols at node 2 and demodulate the received signal at node 1, 3, 4, and 5 to evaluate the SWC performances. We use a PZT stack as the transmission transducer with self-resonant frequency of 40 kHz. The PZT patches were attached to the surface of the pipe as receiving nodes.

The signal processing block diagram is shown in Fig. 12. Where the DUC stands for digital up converter, which convert the baseband signals to passband signals with center frequency of 40 kHz. The transmission symbol rate is 1380 symbols/s. The demodulation results in the lab are shown in Fig. 13. It is shown that the BER increased dramatically after stress wave signals propagating through a join between nodes 3 and 4. This is mainly due to the reflection. Specifically, when stress wave signals propagates from one pipe to another pipe, due to the impedance mismatch in the join, most of the stress wave signals will be reflected back. For this reason, the SNR on node 4 would be much lower than node 3 resulting in a worse BER.

D. Communication Performances Evaluation

The subsea experiment setup is shown in Fig. 14. We directly submerged the testbed into the seawater. Then, we repeated the same testing procedure as what we did in the lab. The testing results are shown in Fig. 15. It turned out that the subsea performances were much better than the lab testing results. Specifically, the error vector magnitude (EVM) in the underwater environment is much smaller than in the lab. To analyze the possible reasons, we show the received signal spectrum in Fig. 16.

The noise in the lab is several decibel higher than subsea at node 4, if we scale the signal strength to the same level. One possible reason could be that the electromagnetic environment in the lab is much more complicated than the subsea environment. The PZT transducer could also act like an EM antenna that may induced some noise into the system. On the other hand, EM waves almost cannot propagate in the seawater. Hence, the subsea EM environment is much more clean than in the lab. Therefore, the SNR of the subsea stress wave signal could be higher than the one in the lab, especially when the received signal is weak.

The noise power at note 3 is quite similar both in the lab or subsea. But there are significant side lobes in the lab environment. One possible reason is that the stress wave reflection in the underwater testbed could be different from the lab testbed. So the CFR would be different. Since subsea performances are

better and the power spectrum is smoother than that in the lab, the reflection in the underwater environment may be smaller than in the air.

VI. CONCLUSION

In the past few decades, thousands of miles of offshore pipelines have been deployed for the transportation of carbon products. Such a huge man made infrastructure network can be potentially utilized as acoustic waveguide for subsea data transmission. The acoustic waveguide in solid mediums such as metallic pipes is also known as stress wave. The theoretical analysis of the propagation of stress wave in this article shows that the attenuation of the single-mode stress wave, e.g., T(0,1)and L(0,1), is extremely small. Although the attenuation factor is proportional to the square of the operation frequency, the amplitude-frequency response of the single-mode stress wave is quite flat if the operation frequencies are within the sub-MHz range. Such a small attenuation property implies that low power and high data rate communication can be potentially achieved for the SWC. For a practical SWC system, the communication bandwidth is highly related to the frequency response of the piezoelectric transducer. The multimode dispersion and strong reflections make the channel response quite frequency selective.

We successfully demonstrated the narrowband SWCs using PZT transducers along steel pipes both in the air and subsea. To further enhance the communication performances and fully utilize the stress wave channel, we need to develop single-mode and wideband acoustic transducer, which will be our future focus on investigating this new paradigm of subsea communication technology.

APPENDIX A

BESSEL FUNCTIONS IN THE SOLUTION OF NAVIER'S EQUATION

To make solutions as concise as possible, two intermediate variables are defined as

$$\begin{cases} \alpha^2 = \frac{\omega^2}{c_l^2} - k^2 \\ \beta^2 = \frac{\omega^2}{c_s^2} - k^2 \end{cases}$$
 (36)

$$f(r) = \begin{cases} A_1 J_0(|\alpha|r) + B_1 Y_0(|\alpha|r), & \omega^2/c_l^2 - k^2 \geqslant 0\\ A_1 I_0(|\alpha|r) + B_1 K_0(|\alpha|r), & \omega^2/c_l^2 - k^2 < 0 \end{cases}$$
(37)

$$\psi_r(r) = \begin{cases} A_2 J_1(|\alpha|r) + B_2 Y_1(|\alpha|r), & \omega^2/c_s^2 - k^2 \geqslant 0 \\ A_2 I_1(|\alpha|r) + B_2 K_1(|\alpha|r), & \omega^2/c_s^2 - k^2 < 0 \end{cases}$$
(38)

$$\psi_{\theta}(r) = \begin{cases} A_3 J_1(|\alpha|r) + B_3 Y_1(|\alpha|r), & \omega^2/c_s^2 - k^2 \geqslant 0\\ A_3 I_1(|\alpha|r) + B_3 K_1(|\alpha|r), & \omega^2/c_s^2 - k^2 < 0 \end{cases}$$
(39)

$$\psi_z(r) = \begin{cases} A_4 J_0(|\alpha|r) + B_4 Y_0(|\alpha|r), & \omega^2/c_s^2 - k^2 \geqslant 0\\ A_4 I_0(|\alpha|r) + B_4 K_0(|\alpha|r), & \omega^2/c_s^2 - k^2 < 0. \end{cases}$$
(40)

In (37)–(40), A_i and B_i , i=1,2,3, and 4, are arbitrary constants. J_{ν} and I_{ν} are first kind Bessel functions, Y_{ν} and K_{ν}

are second kind Bessel functions, and ν is the order of Bessel function.

ACKNOWLEDGMENT

Potential Conflict of Interests: G. Song holds financial interest in AEM, a startup company in structural health monitoring.

REFERENCES

- M. J. Kaiser, "Offshore pipeline construction cost in the US Gulf of Mexico," Mar. Policy, vol. 82, pp. 147–166, 2017.
- [2] A. Wu, S. He, Y. Ren, N. Wang, S. C. M. Ho, and G. Song, "Design of a new stress wave-based pulse position modulation (PPM) communication system with piezoceramic transducers," *Sensors*, vol. 19, no. 3, 2019, Art. no. 558.
- [3] Q. Ji, "Stress wave communication and waveform design for energy charging in solid structures," Ph.D. dissertation, Dept. Mech. Eng., Univ. Houston, Houston, TX, USA, 2016.
- [4] B. Gulbahar and O. B. Akan, "A communication theoretical modeling and analysis of underwater magneto-inductive wireless channels," *IEEE Trans. Wireless Commun.*, vol. 11, no. 9, pp. 3326–3334, Sep. 2012.
- [5] H. Guo, Z. Sun, and P. Wang, "Channel modeling of MI underwater communication using tri-directional coil antenna," in *Proc. IEEE Global Commun. Conf.*, 2015, pp. 1–6.
- [6] D. Wei et al., "Exploiting magnetic field analysis to characterize MI wireless communications in subsea environments," in Proc. Int. Conf. Comput., Netw., Commun., 2018, pp. 805–809.
- [7] D. Wei et al., "Ferrite assisted geometry-conformal magnetic induction antenna and subsea communications for AUVs," in Proc. IEEE Global Commun. Conf., 2018, pp. 1–6.
- [8] D. Wei, S. S. Soto, J. Garcia, A. T. Becker, L. Wang, and M. Pan, "ROV assisted magnetic induction communication field tests in underwater environments," in *Proc. 13th ACM Int. Conf. Underwater Netw. Syst.*. ACM, pp. 1–5, 2018, Art. no. 20.
- [9] D. S. Drumheller, "Acoustical properties of drill strings," J. Acoust. Soc. Amer., vol. 85, no. 3, pp. 1048–1064, 1989.
- [10] C. C. Johnson, "A seismic communications investigation employing a piezoelectric transducer," Southwest Res. Inst., San Antonio, TX, USA, Tech. Rep. AD0752218, 1972.
- [11] T. J. Lawry et al., "Penetration-free system for transmission of data and power through solid metal barriers," in *Proc. Mil. Commun. Conf.*, 2011, pp. 389–395.
- [12] S. Siu, Q. Ji, W. Wu, G. Song, and Z. Ding, "Stress wave communication in concrete: I. Characterization of a smart aggregate based concrete channel," *Smart Mater. Struct.*, vol. 23, no. 12, 2014, Art. no. 125030.
- [13] S. Siu, J. Qing, K. Wang, G. Song, and Z. Ding, "Stress wave communication in concrete: II. Evaluation of low voltage concrete stress wave communications utilizing spectrally efficient modulation schemes with PZT transducers," Smart Mater. Struct., vol. 23, no. 12, 2014, Art. no. 125031.
- [14] Q. Ji, M. Ho, R. Zheng, Z. Ding, and G. Song, "An exploratory study of stress wave communication in concrete structures," *Smart Struct. Syst.*, vol. 15, no. 1, pp. 135–150, 2015.
- [15] D. Alleyne, B. Pavlakovic, M. Lowe, and P. Cawley, "Rapid, long range inspection of chemical plant pipework using guided waves," AIP Conf. Proc., vol. 557, no. 1,, pp. 180–187, 2001.
- [16] M. Sheard, "Field experience of using long-range ultrasonic testing," *Insight*, vol. 43, no. 2, pp. 73–83, 2001.
- [17] E. Leinov, M. J. Lowe, and P. Cawley, "Ultrasonic isolation of buried pipes," *J. Sound Vib.*, vol. 363, pp. 225–239, 2016.
- [18] L. Gao, W. R. Gardner, C. Robbins, D. H. Johnson, and M. Memarzadeh, "Limits on data communication along the drillstring using acoustic waves," SPE Reserv. Eval. Eng., vol. 11, no. 1, pp. 141–146, 2008.
- [19] M. A. Gutierrez-Estevez et al., "Acoustic broadband communications over deep drill strings using adaptive OFDM," in Proc. IEEE Wireless Commun. Netw. Conf., 2013, pp. 4089–4094.
- [20] D. Ma, Y. Shi, W. Zhang, and G. Liu, "Design of acoustic transmission along drill strings for logging while drilling data based on adaptive NC-OFDM," AEU—Int. J. Electron. Commun., vol. 83, pp. 329–338, 2018.
- [21] M. Memarzadeh, "Optimal borehole communication using multicarrier modulation," Ph.D. dissertation, Rice Univ., Houston, TX, USA, 2007.

- [22] P. Li, H. Gu, G. Song, R. Zheng, and Y. Mo, "Concrete structural health monitoring using piezoceramic-based wireless sensor networks," *Smart Struct. Syst.*, vol. 6, no. 5/6, pp. 731–748, 2010.
 [23] N. Hoult, P. Fidler, and C. Middleton, "Wireless structural health mon-
- [23] N. Hoult, P. Fidler, and C. Middleton, "Wireless structural health monitoring of bridges: Current challenges and future innovations," in *Proc. AustRoads Bridge Conf.*, 2009, pp. 1–12.
- [24] S. Kailaswar et al., "Concretecom: A new communication paradigm for building structural health monitoring," in Proc. 4th ACM Workshop Embedded Sens. Syst. Energy-Efficiency Buildings, 2012, pp. 131–137.
- [25] M. Chitre, S. Shahabudeen, and M. Stojanovic, "Underwater acoustic communications and networking: Recent advances and future challenges," *Mar. Technol. Soc. J.*, vol. 42, no. 1, pp. 103–116, 2008.
- [26] I. F. Akyildiz, D. Pompili, and T. Melodia, "Underwater acoustic sensor networks: Research challenges," *Ad hoc Netw.*, vol. 3, no. 3, pp. 257–279, 2005
- [27] C. Jun-Hong, K. Jiejun, M. Gerla, and Z. Shengli, "The challenges of building mobile underwater wireless networks for aquatic applications," *Network*, vol. 20, no. 3, pp. 12–18, 2006.
- [28] L. Lanbo, Z. Shengli, and C. Jun-Hong, "Prospects and problems of wireless communication for underwater sensor networks," Wireless Commun. Mobile Comput., vol. 8, no. 8, pp. 977–994, 2008.
- [29] A. Song, M. Badiey, H. Song, and W. Hodgkiss, "Impact of source depth on coherent underwater acoustic communications," *J. Acoust. Soc. Amer.*, vol. 128, no. 2, pp. 555–558, 2010.
- [30] D. Wei, C. Qi, J. Chen, A. Song, G. Song, and M. Pan, "Pipe data through the water: Stress wave communications along pipelines," in *Proc. Int. Conf. Underwater Netw. Syst.*, 2019, pp. 1–5.
- [31] J. L. Rose, Ultrasonic Guided Waves in Solid Media. Cambridge, U.K.: Cambridge Univ. Press, 2014.
- [32] D. M. Pozar, Microwave Engineering, 4th ed. Hoboken, NJ, USA: Wiley, 2011
- [33] P. Bocchini, A. Marzani, and E. Viola, "Graphical user interface for guided acoustic waves," *J. Comput. Civil Eng.*, vol. 25, no. 3, pp. 202–210, 2010
- [34] E. Leinov, M. J. Lowe, and P. Cawley, "Investigation of guided wave propagation and attenuation in pipe buried in sand," *J. Sound Vib.*, vol. 347, pp. 96–114, 2015.
- [35] D. Alleyne and P. Cawley, "The excitation of lamb waves in pipes using dry-coupled Piezoelectric transducers," *J. Nondestruct. Eval.*, vol. 15, no. 1, pp. 11–20, 1996.
- [36] O. Karpenko, Signal Analysis in Guided Wave Structural Health Monitoring. East Lansing, MI, USA: Michigan State Univ., 2013.
- [37] Q. Kong, R. H. Robert, P. Silva, and Y. Mo, "Cyclic crack monitoring of a reinforced concrete column under simulated pseudo-dynamic loading using Piezoceramic-based smart aggregates," Appl. Sci., vol. 6, no. 11, 2016, Art. no. 341.
- [38] T. Jiang, Q. Kong, D. Patil, Z. Luo, L. Huo, and G. Song, "Detection of debonding between fiber reinforced polymer bar and concrete structure using Piezoceramic transducers and wavelet packet analysis," *IEEE Sensors* J., vol. 17, no. 7, pp. 1992–1998, Apr. 2017.
- [39] Q. Ji, Z. Ding, N. Wang, M. Pan, and G. Song, "A novel waveform optimization scheme for piezoelectric sensors wire-free charging in the tightly insulated environment," *IEEE Internet Things J.*, vol. 5, no. 3, pp. 1936–1946, Jun. 2018.
- [40] Y. Xu, M. Luo, Q. Liu, G. Du, and G. Song, "PZT transducer array enabled pipeline defect locating based on time-reversal method and matching pursuit de-noising," Smart Mater. Struct., vol. 28, no. 7, 2019, Art. no. 075019.
- [41] A. V. Carazo, Novel Piezoelectric Transducers for High Voltage Measurements. Barcelona, Spain: Universitat Politècnica de Catalunya, 2000.



Debing Wei (Student Member, IEEE) received the B.S. and M.S. degrees in electrical engineering from North China Electric Power University, Baoding, China, in 2008 and 2011, respectively. He is currently working toward the Ph.D. degree in electrical and computer engineering with the University of Houston, Houston, TX, USA.

His current research interests include underwater MI wireless communications, stress wave communications, and underwater hybrid networking.



Chaoxian Qi (Student Member, IEEE) received the B.S. degree in electric engineering from the University of Electric Science and Technology of China, Chengdu, China, in 2017. He is currently working toward the Ph.D. degree in electrical and computer engineering with the University of Houston, Houston, TX, USA.

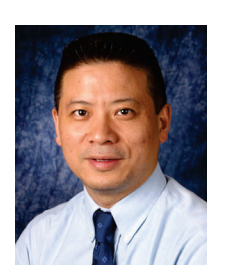
His research interests include numerical modeling in electromagnetics and acoustics, subsurface and subsea wireless communication, and inverse source problem.



munications.

Chenpei Huang (Student Member, IEEE) received the B.S. degree in electronic information engineering from the School of Electronic Engineering, University of Electronic Science and Technology of China, Chengdu, China, in 2019. He is currently working toward the Ph.D. degree in electrical and computer engineering with the Department of Electrical and Computer Engineering, University of Houston, Houston, TX, USA.

His research interests include underwater communications and networking and the stress wave com-



Gangbing Song (Member, IEEE) received the B.S. degree in mechanical engineering from Zhejiang University, Hangzhou, China, in 1989, and the M.S. and Ph.D. degrees in mechanical engineering from the Department of Mechanical Engineering, Columbia University in the City of New York, New York, NY, USA, in 1991 and 1995, respectively.

He is the founding Director of the Smart Materials and Structures Laboratory and a Professor of Mechanical Engineering with the University of Houston, Houston, TX, USA. He has expertise in smart

materials and structures, structural vibration control, piezoceramics, ultrasonic transducers, structural health monitoring, and damage detection. He has developed two new courses in smart materials and authored/coauthored more than 500 papers, including 379 peer-reviewed journal articles. He is also an inventor or coinventor of 24 U.S. patents.

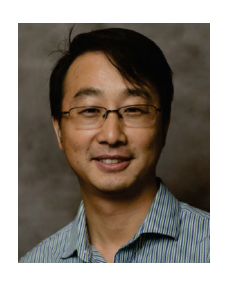
Dr. Song was a recipient of the NSF CAREER award in 2001. He has received research funding in smart materials and related research from NSF, DoE, NASA, Department of Education, Texas Higher Education Board, TSGC, UTMB, OSGC, OAI, ODoT, HP, OptiSolar, GE, and Cameron. He is a recipient of the prestigious Outstanding Technical Contribution Award from the Aerospace Division of ASCE, the Excellence in Research & Scholarship Award at Full Professor Level from UH, Celebrating Excellence Award for Excellence in Education from ISA, the IEEE Educational Activities Board Meritorious Achievement Award in Informal Education. He is a member of ASCE and ASME. He was the General Chair of the Earth and Space Conference 2010, Aerospace Division, ASCE.



Jiefu Chen (Senior Member, IEEE) received the B.S. degree in engineering mechanics and the M.S. degree in dynamics and control from the Dalian University of Technology, Dalian, China, in 2003, and the Ph.D. degree in electrical engineering from Duke University, Durham, NC, USA, in 2006 and 2010, respectively.

From 2011 to 2015, he was a Staff Scientist with the Advantage Research and Development Center, Weatherford International, Ltd., Houston, TX, USA. Since September 2015, he has been an Assistant Pro-

fessor with the Department of Electrical and Computer Engineering, University of Houston, Houston, TX, USA. His research interests include computational electromagnetics, inverse problems, machine learning for scientific computing, oilfield data analytics, seismic data processing, underground and underwater wireless communication, and well logging.



Aijun Song (Member, IEEE) received the Ph.D. degree in electrical engineering from the Department of Electrical Engineering, University of Delaware, Newark, Delaware, in 2005.

He is currently an Assistant Professor with the Department of Electrical and Computer Engineering, University of Alabama, Tuscaloosa, AL, USA. From 2005 to 2008, he was a Postdoctoral Research Associate with the College of Earth, Ocean and Environment, University of Delaware, Newark, DE. During this period, he was also an Office of Naval Research

(ONR) Postdoctoral Fellow, supported by the Special Research Award in the ONR Ocean Acoustics program. He was an Assistant Research Professor with the University of Delaware, Newark, DE, USA, from 2008 to 2014, and an Associate Research Professor from 2014 to 2015. His current research interests include digital communications and signal processing techniques for radio-frequency and underwater acoustic channels, ocean acoustics, sensor networks, and ocean monitoring and exploration.

Dr. Song was the General Co-Chair of 2018 March NSF Workshop on Underwater Wireless Communications and Networking and 2018 November NSF Workshop on Underwater Wireless Infrastructure. He was the General Co-Chair of the 14th International Conference on Underwater Networks & Systems. He was the recipient of the National Science Foundation CAREER Award in 2021.



Miao Pan (Senior Member, IEEE) received the B.Sc. degree in electrical engineering from the Dalian University of Technology, Dalian, China, in 2004, the M.A.Sc. degree in electrical and computer engineering from the Beijing University of Posts and Telecommunications, Beijing, China, in 2007, and the Ph.D. degree in electrical and computer engineering from the University of Florida, Gainesville, FL, USA, in 2012.

He is currently an Associate Professor with the Department of Electrical and Computer Engineering,

University of Houston, Houston, TX, USA. His research interests include wireless/AI for AI/wireless, deep learning privacy, cybersecurity, underwater communications and networking, and cyber-physical systems.

Dr. Pan was a recipient of NSF CAREER Award in 2014. His work won IEEE TCGCC Best Conference Paper Awards 2019, Best Paper Awards in ICC 2019, VTC 2018, Globecom 2017, and Globecom 2015. He is an Editor for IEEE OPEN JOURNAL OF VEHICULAR TECHNOLOGY and an Associate Editor for IEEE INTERNET OF THINGS (IOT) JOURNAL (Area 5: Artificial Intelligence for IoT), and was an Associate Editor for IEEE INTERNET OF THINGS (IOT) JOURNAL (Area 4: Services, Applications, and Other Topics for IoT) from 2015 to 2018. He has also been a Technical Organizing Committee for several conferences such as a TPC Co-Chair for Mobiquitous 2019 and ACM WUWNet 2019. He is a member of AAAI and ACM.